АТОМНА ЕНЕРГЕТИКА
ATOMIC ENERGY

УДК 621.039.546+621.039.58 https://doi.org/10.15407/jnpae2024.03.257

H. Aboud[1,*], I. T. Al-Alawy[1,2]

[1] *Physics Department, College of Science, Mustansiriyah University, Baghdad, Iraq*
[2] *Department of Medical Physics, College of Medical Health Technology, Alshaab University, Baghdad, Iraq*

*Corresponding author: han55608@yahoo.com

RADIATION SHIELDING, DOSE RATE AND STOPPING POWER OF CADMIUM - BISMUTH - LEAD - ZINC - BORATE GLASS SYSTEM: INFLUENCE OF Bi_2O_3 DOPING

Glass systems of the form (70-x)B_2O_3-10ZnO-10PbO-10CdO-xBi_2O_3 (with x = 0 to 20 mol%) were prepared by the standard melt-quenching approach and characterized. The role of varying Bi_2O_3 doping contents on the radiation shielding, dose rate, and stopping power of the proposed glasses was examined. Various radiation shielding properties, such as exposure buildup factors, gamma-ray constants and dose rates, and total neutron removal cross-section, were estimated. The x-ray diffractometer patterns of the samples showed their amorphous characteristics. Glass density was increased from 5.34 to 6.95 g/cm^3, and the energy band gap was reduced with the increase in Bi_2O_3 doping contents. In addition, both mass attenuation numbers and effective atomic numbers of the samples (calculated using Phy-X software) in the gamma-ray energy range of 0.015 to 15 MeV were increased with the increase in Bi_2O_3 contents. With the increase in Bi_2O_3 doping, the gamma-ray shielding, stopping power, and neutron removal cross-section of the glasses were improved. This new glass composition was asserted to be a good candidate for radiation shielding applications.

Keywords: gamma-radiation shielding, borate glass, neutrons cross sections, attenuation parameters.

1. Introduction

Nowadays, there is a great demand for cost-effective and good-quality radiation shielding materials for attenuating hazardous gamma-ray radiation from different sources to the safety limit. The shield design criteria are usually based on lessening the probability of harmful ionizing radiation entering the living matter [1 - 3]. Since ionizing radiation plays a crucial role in shielding considerations, it is essential to clearly understand from the beginning what is meant by this form of radiation and its subsequent protection [4, 5]. The determination of the nature, strength, energy, and spatial distributions of the influential sources of radiation is a necessary undertaking at an early stage of any shielding calculation. The attenuation coefficient of high-energy photons is determined by energy and atomic number (Z)-dependent combined mechanisms like the Compton interaction, photo-electric effect, and pair productions. The pair productions and photo absorptions are regarded as the total photon removal mechanisms, while the Compton scattering decelerates the photons, removing energy via the absorptions of photons [6, 7].

Over the years, for efficient gamma-ray shielding, various types of glass, polymer, alloy, ceramic, clay, and brick were implemented [8 - 12]. Glasses and ceramics made of tellurite, germanate, phosphate, borate, tungstate, and silicate, owing to their easy synthesis and high transparency, have been intensively studied for gamma-ray shielding applications [13 - 17]. In addition, these glass systems show excellent chemical, mechanical, and thermal stability, low melting temperatures and viscosities, high heat resistance, and durability, thus making them suitable for efficient radiation shielding purposes [18]. It was shown that the incorporation of PbO into borate-based glass systems can appreciably reduce photon energy, thus improving their overall radiation shielding properties [19]. Glasses containing heavy metals (like PbO, WO, TeO, etc.) reveal relatively stronger nonlinear properties, making them promising for optical devices such as power limiters and switches. In addition, PbO, due to its very high density, possesses a low half-value layer when doped to any glass or ceramic system in an appropriate quantity, making them effective as radiation shields [20]. Despite many efforts, a glass-based radiation shielding material with excellent mass attenuation coefficient (MAC), equivalent atomic number (Z_{eq}), photon build-up exposure factor (BEF), dose rate, total neutron removal cross-section ($\sum R$), and stopping power is far from being obtained.

Considering the practical importance of high-performance radiation shielding materials, a series of cadmium - bismuth - lead - zinc - borate glasses were prepared at various Bi_2O_3 doping contents and analyzed using different techniques. We looked at how different amounts of Bi_2O_3 affected the radiation shielding parameters, dose rate, MAC (μ/ρ), and stopping power of the proposed glasses to see how well they blocked gamma-rays. Phy-X software was used to calculate all the parameters to complement the experimentally measured ones.

2. Experimental

2.1. Glass synthesis

Five samples with the nominal composition of xBi_2O_3-10CdO-10ZnO-10PbO-(70-x)B_2O_3 (with x = 0 to 20 mol%) were produced by the melt-quenching method. Pure (99.99 % purity) glass constituents (in powder form) were purchased from Sigma-Aldrich Company and used without further chemical treatment. A total of about 10 g (called batch mixture) of the powder constituents were weighed and mixed via milling (for 1 h) to get a uniform blend. The mixture was kept in an alumina crucible and then melted in a furnace at 950 ºC (for 2 h). The melt was constantly stirred to get a homogeneous mix and later transferred to a pre-heated steel mold with rapid pressing by another steel shield. Next, the mold containing the pressed mix was subjected to thermal annealing at 400 ºC (for 3 h). A part of the frozen solid from each batch sample was crushed for the x-ray diffractometer (XRD) analyses. Utilizing a Rigaku MiniFlex II XRD, the amorphous character of the produced samples was examined. A UV-Vis-NIR Agilent 8453 absorption spectrophotometer was used to capture the glasses' room temperature absorption and reflection spectra in the 200 - 2000 nm wavelength range. All the characterizations were conducted at room temperature. The density of each sample ρ_g was measured three times by the Archimedes approach with pure (99.99 %) toluene as an immersion liquid:

$$\rho_g = \frac{W_a}{W_a - W_b}\rho_t, \tag{1}$$

where W_a and W_b are the corresponding sample's weight in air and in toluene of density ρ_t = 0.865 g/cm^3.

2.2. Theoretical

Mass attenuation coefficient (*MAC*).

For any radiation shielding material, it is important to measure the values of μ/ρ to determine its incident radiation absorption capacity [21 - 23]. The values of μ/ρ for the proposed glass system were calculated in terms of their partial density (W_i) using [24 - 26]:

$$\frac{\mu}{\rho} = \sum_i W_i \left(\frac{\mu}{\rho}\right)_i. \tag{2}$$

Photon exposure build-up factor (*EBFs*).

The photon EBFs of the glasses were evaluated using the interpolation method in terms of Z_{eq} [27 - 29].

Gamma-factor or specific gamma-ray constant (Γ).

To estimate the values of Γ for the studied glasses, a photon source of 1 Ci activity was kept at a distance of 1 m and exposed at a rate of *R*/*h* [30] using the relation:

$$\Gamma = 657.68 \cdot E_\gamma \frac{\mu_{en}}{\rho}\left(\frac{R\,m^2}{Ci \cdot h}\right). \tag{3}$$

Irradiation dose (*D*).

The values of *D* were estimated in terms of the radioactive source distance (*r*, m), activity (*A*, Bq), and net exposure time (*t*, h) using [31]:

$$D = \Gamma \cdot A \frac{t}{r^2}. \tag{4}$$

Total neutron removal cross-section ($\sum R$).

For fast neutron attenuation in a homogeneous shielding material, the concept of $\sum R$ is important. In this work, for the glasses made of different constituents, the corresponding effective removal cross-section was calculated via [32, 33]:

$$\sum R = \sum_i W_i \left(\sum \frac{R}{\rho}\right)_i. \tag{5}$$

The Phy-X program was used to determine the values of Z_{eq} [34], and radiation attenuation parameters such as the scattering length and absorption cross-section for the glasses. In addition, the coherent (b_{coh}) and incoherent (b_{inc}) scattering length and absorption (σ_{abs}), coherent (σ_{coh}), incoherent (σ_{inc}), and total (σ_{tot}) scattering cross-section of neutrons were calculated. The neutron shielding parameter (NSP) of the glasses was evaluated in terms of the mass fraction (f_i) of the *i*-th element in each glass via [35]. Lastly, the mass stopping power (MSP) was calculated using the SRIM code.

$$(NSP)_{Compound} = \sum_i f_i (NSP)_i. \tag{6}$$

3. Results and discussion

Table 1 furnishes the detailed composition, sample code (S1 to S5), density, and band gap energy of the glasses. Fig. 1 shows the XRD profiles of the prepared glasses. The broad halo without any prominent diffraction peaks in the XRD pattern of the as-quenched samples indicated a glassy nature. The densities of the samples were increased (5.34 to 6.95 g/cm^3) and the band gap energies were decreased (2.75 to 2.60 eV) with the increase in Bi_2O_3 doping contents. This was mainly due to the changes in the glass network structures due to the reduction in the number of metal-oxide bonds and the increase of non-bridging oxygen (NBO) [36].

Table 1. **Composition, sample code, density, and band gap energy of the glasses**

Composition, mol%							
Sample codes	B_2O_3	CdO	PbO	ZnO	Bi_2O_3	Density, g/cm^3	Eg, eV
S1	70	10	10	10	0	5.34	2.75
S2	65	10	10	10	5	5.92	2.70
S3	60	10	10	10	10	6.23	2.68
S4	55	10	10	10	15	6.54	2.62
S5	50	10	10	10	20	6.95	2.60

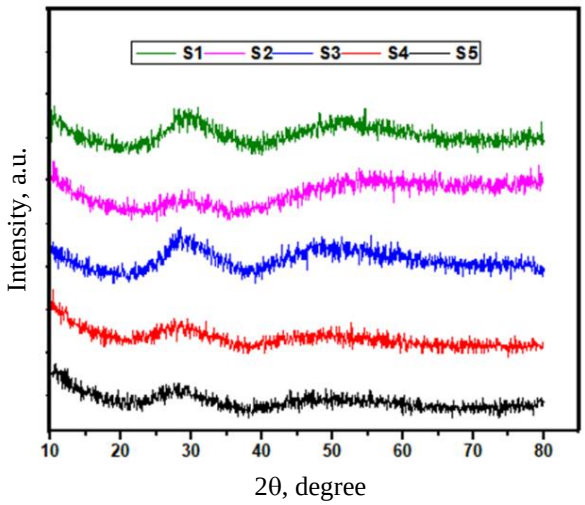

Fig. 1. XRD profiles of produced glasses. (See color Figure on the journal website.)

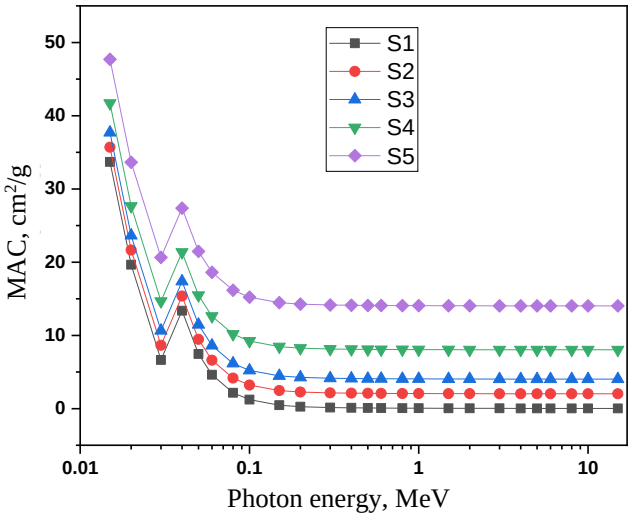

Fig. 2. Photon energy-dependent variation of MAC of the prepared samples. (See color Figure on the journal website.)

Fig. 2 illustrates the incident gamma-ray photon energy (E) dependent values of μ/ρ of the glasses, which were observed to be highest at low energy, and the values were dropped with the increase in energy of photons. Beyond 5 MeV, the values μ/ρ of the glasses insignificantly depended on the energy of the incident photon, which was primarily due to the partial interactions of the photons with the material. At both low and high energies, sample S5 produced the highest equivalent MAC. In the lower energy region (0.015 - 0.04 MeV), the photoelectric effect was the primary interaction mechanism (~1/E^3). In the middle energy region (0.04 to 3 MeV), the Compton scattering process was the major interaction mechanism (~1/E). Conversely, in the higher energy region (3 - 10 MeV), the pair production process was the dominant interaction mechanism (~log E) [37, 38].

Fig. 3 shows the photon energy (0.015 to 15 MeV) dependent values of Z_{eq} for the studied samples. In the lower energy region, the values of Z_{eq} of the glasses were augmented a little, reached a maximum, and then dropped. However, beyond 3 MeV, the Z_{eq} values almost remain constant due to the dominant pair production mechanism. The observed maximum of Z_{eq} at lower photon energy can be attributed to the predominance of the photoelectric effect in the electronic K-shell of heavy metals like cadmium, bismuth, and zinc. In fact, the contents of the dopants played a significant role in the variation of the Z_{eq} values of the glasses.

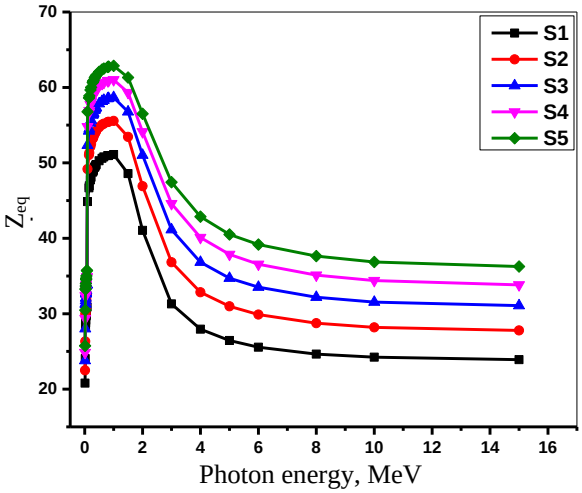

Fig. 3. Photon energy-dependent variation of Z_{eq} of the glasses. (See color Figure on the journal website.)

Fig. 4 shows the photon energy-dependent variation of the EBF for sample S5, which ranged from 1 to 15 mfp, indicating an improvement in the depth of penetration. The obtained lowest value of EBF at 0.1 MeV can be attributed to the dominance of the photoelectric interaction mechanism in the sample. Beyond 0.2 MeV (intermediate energies), the EBF

values increased with the increase of energy and attained a maximum, which was mainly due to the predominant Compton scattering process. Above 2.0 MeV, the pair production process became more dominant than Compton scattering, reducing the values of the EBF of the glasses [39, 40].

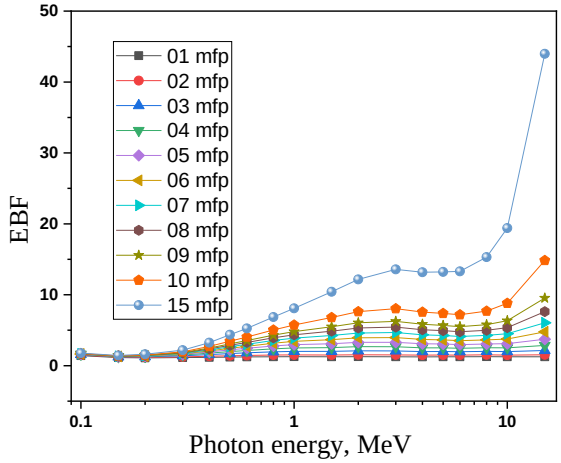

Fig. 4. Photon energy-dependent variation of EBF for sample S5. (See color Figure on the journal website.)

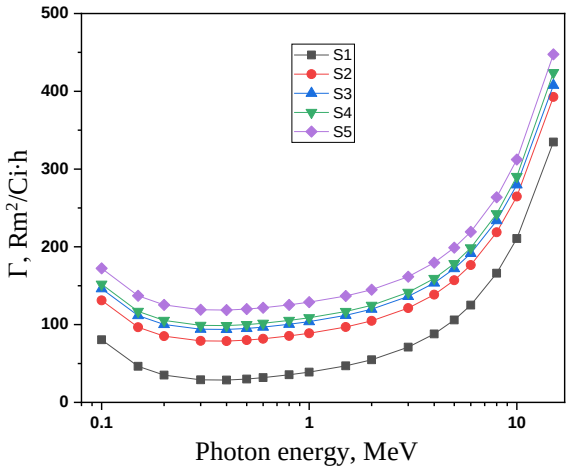

Fig. 5. Photon energy-dependent variation of Γ of the glasses. (See color Figure on the journal website.)

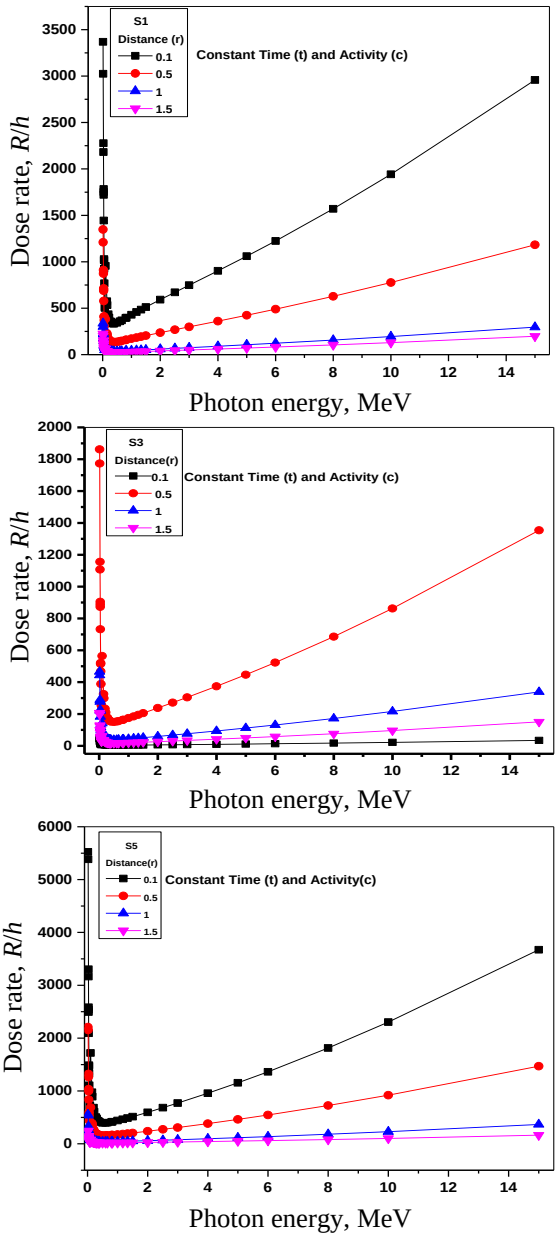

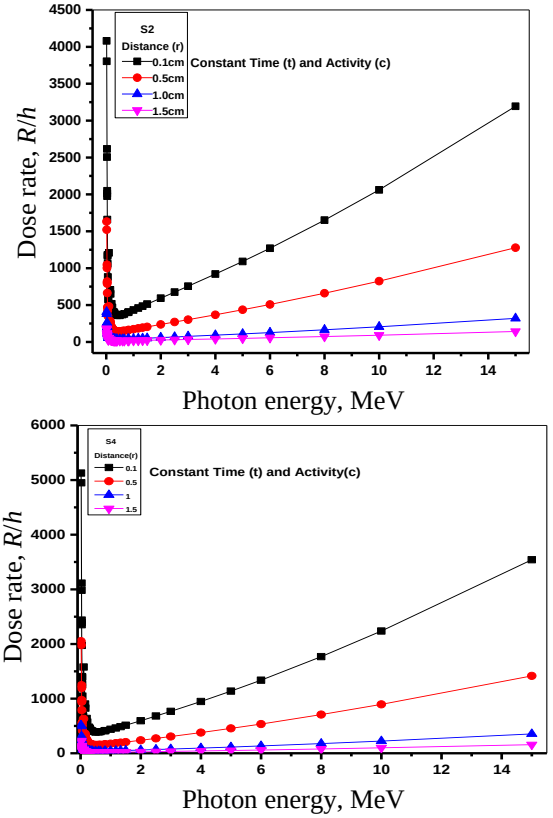

Fig. 6. Photon energy-dependent variation of R/h of the glasses at different distances. (See color Figure on the journal website.)

Fig. 5 displays the photon energy-dependent variation of Γ of the glasses. In this work, we determined the Γ by utilizing theoretical calculations. All glasses showed comparable behavior, wherein the values of Γ were increased with the increase of incident photon energies. At low energy, the Γ values reduce up to 0.4 MeV related to the photoelectric effect interaction's dominance. Then, the Γ values increase progressively up to 15 MeV attributed to the occurrence of the Compton and pair production interaction. In addition, the values of Γ were gradually increased with the increase in Bi_2O_3 doping contents.

The glass sample dosage rate (R/h) was computed theoretically. Fig. 6 presents the photon energy-dependent changes in the gamma-dose rate (R/hr) of the glasses at different distances from the radiation source. The values of dose rate decreased with the increase in glass thickness, wherein sample S5 made with 20 wt% of Bi_2O_3 doping yielded the best value of dose rate, indicating its potential for gamma-radiation shielding applications.

Fig. 7 shows the neutron removal cross-section of the samples S1 and S5 compared to other concretes.

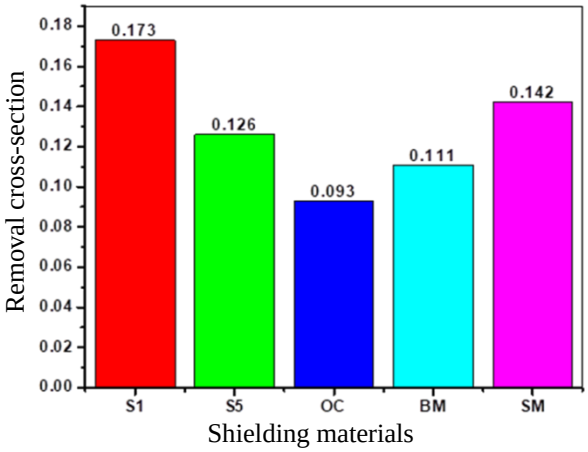

Fig. 7. The removal cross-section of samples S1 and S5 compared to SM, BM, and OC.
(See color Figure on the journal website.)

Table 2. **Fast neutrons effective and mass removal cross-section of the glasses**

Sample code	Element	Weight fraction	Partial density	$\sum R/\rho$, cm^2g^{-1}	Manual	Removal cross-section $\sum R$, cm^{-1} Phy-X	(%RD)
S1	H	0.0212	0.0848	0.598	0.171	0.173	1.169 %
	B	0.0758	0.3032	0.0575			
	O	0.481	1.924	0.0405			
	Cd	0.1127	0.4508	0.014			
	C	0.0361	0.1444	0.0502			
	Pb	0.2076	0.8304	0.0104			
	Zn	0.0655	0.262	0.0183			
S2	H	0.0176	0.0704	0.598	0.157	0.158	0.636 %
	B	0.0629	0.2516	0.0575			
	O	0.4439	1.7756	0.0405			
	Cd	0.1006	0.4024	0.014			
	C	0.0376	0.1504	0.0502			
	Pb	0.1854	0.7416	0.0104			
	Bi	0.0585	0.234	0.0103			
S3	H	0.0147	0.0588	0.598	0.143	0.145	1.39 %
	B	0.524	0.2096	0.0575			
	O	0.4139	1.6556	0.0405			
	Cd	0.0909	0.3636	0.014			
	C	0.0388	0.1552	0.0502			
	Pb	0.1675	0.67	0.0104			
	Bi	0.0529	0.2116	0.0103			
S4	H	0.0123	0.049	0.598	0.132	0.134	1.51 %
	B	0.0438	0.1753	0.0575			
	O	0.3892	1.5567	0.0405			
	Cd	0.0829	0.3314	0.014			
	C	0.1527	0.1593	0.0502			
	Pb	0.0482	0.6109	0.0104			
	Bi	0.0102	0.1928	0.0103			
S5	H	0.0366	0.0409	0.598	0.123	0.126	2.43 %
	B	0.3685	0.1464	0.0575			
	O	0.0762	1.474	0.0405			
	Cd	0.0407	0.3046	0.014			
	C	0.1404	0.1627	0.0502			
	Pb	0.0443	0.5614	0.0104			
	Bi	0.0443	0.1771	0.0103			

Table 2 summarizes the manual calculation and Phy-X program values of the removal cross-section of fast neutrons for the glasses. There was good compatibility between the two processes, as indicated by the percentage relative difference (%RD). The values of $\sum R$ for S1, S2, S3, S4, and S5 samples were 0.173, 0.157, 0.154, 0.134, and 0.126 cm^{-1}, respectively. These values closely agreed with those obtained due to the increase in Bi_2O_3 contents. The present glasses indicate a decrease from S1 to S5, and S1 is the maximum value of the glass sample. This is attributed to the spontaneous improvement of the Bi_2O_3 weight fraction at the expense of B and O. In addition, Bi_2O_3 had a lower $\sum R$ compared to B and O (see Table 2). In fact, the quantity of elements with lower atomic numbers, like B and O as glass constituents was responsible for the decrease in $\sum R$ values. Some studies revealed that low atomic number elements demonstrate higher neutron shielding capacity. Sample S1 showed optimum results, which are much higher compared to the commercially available steel magnetite (SM = 0.142 cm^{-1}), basalt (BM = 0.111 cm^{-1}), and ordinary concrete (OC = = 0.093 cm^{-1}) [41, 42].

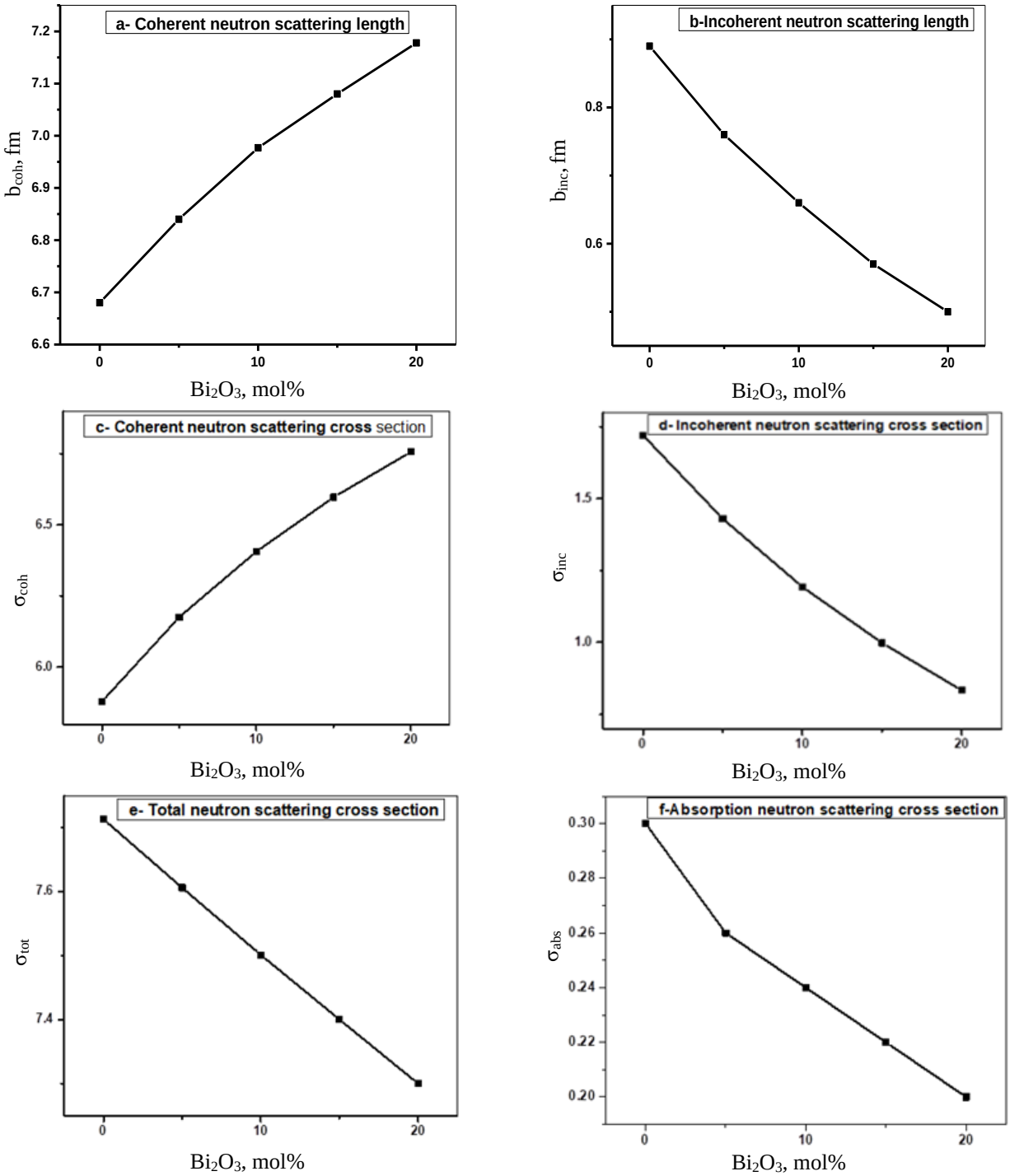

Fig. 8. Bi_2O_3 contents-dependent variation of b_{coh}, b_{inc}, σ_{coh}, σ_{inc}, σ_{tot}, and σ_{abs} of the glasses.

Fig. 8 depicts the content-dependent variation of different NSP values like b_{coh}, b_{inc}, σ_{coh}, σ_{inc}, σ_{tot}, and σ_{abs} of the glasses. Except σ_{coh} and b_{coh} all other values decreased with the increase in Bi_2O_3 contents, indicating the significant role of dopants in changing the glass network structures and various interaction mechanisms.

These results are consistent with the previous findings reported in the literature [43, 44].

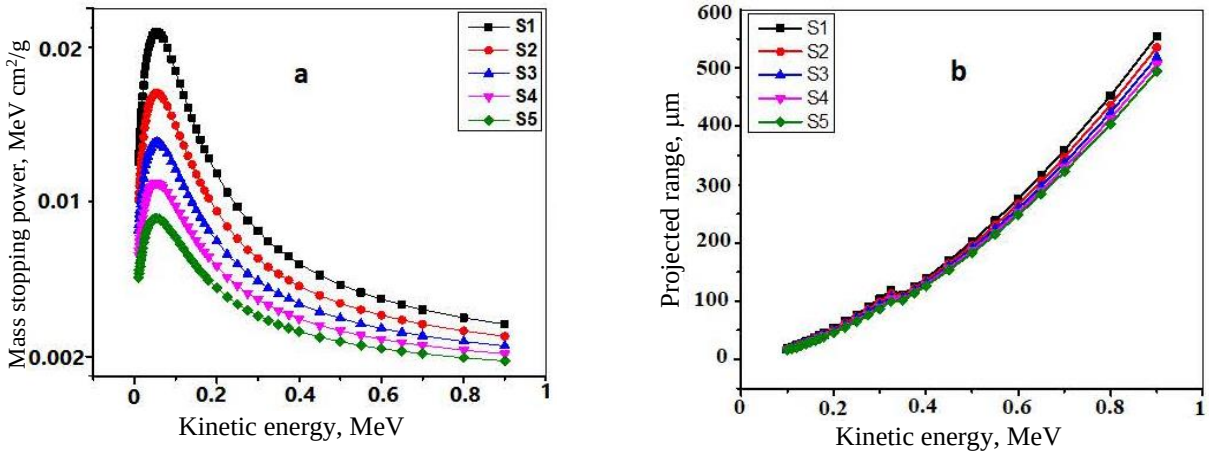

Fig. 9. Protons kinetic energy-dependent variation of the MSP and projected range of the glasses. (See color Figure on the journal website.)

Fig. 9 displays the kinetic energy-dependent variation of the MSP and the projected range of the glasses. The values of MSP in the energy range 0.01 - 1 MeV (see Fig. 9, *a*) were increased to attain the highest at 0.1 MeV and then decreased with the increase of kinetic energy. This observation can be attributed to the atomic excitations and ionizations in the path of incident protons [45]. The glass containing Bi_2O_3 of 20 wt% showed the lowest MSP for the incident protons energy. However, the values of the projected range (see Fig. 9, *b*) steadily increased with the increase in incident protons energy, indicating the retardation of the protons due to strong interaction with the heavy elements in the glasses. It was asserted that the proposed glass composition is suitable for effective radiation shielding purposes. Moreover, the projected range decreased with the increase in Bi_2O_3 doping contents because of the improvement in Z_{eff} values of the glasses [46].

4. Conclusion

New types of borate glasses were composed using the melt-quenching method and characterized to see their radiation shielding potency. Based on the experimental and theoretical results and analyses, the following conclusions are drawn:

– The proposed samples showed an amorphous character obtained from XRD analyses.

– Glass densities increased with the increase in Bi_2O_3 doping levels.

– The band gap energies of the glasses were reduced from 2.75 - 2.60 eV with the increase in Bi_2O_3 doping levels, which was due to the increase of NBO and glass network structures.

– The radiation shielding parameters in the energy range of 3 - 10 MeV of the glasses obtained using Phy-X software showed a decrease in the (μ/ρ) values with the increase of incident energy and Bi_2O_3 doping levels.

– The values of EBF estimated in the range of 0.015 to 15 MeV showed the penetration depth between 1 to 15 mfp.

– The values of MSP and projected range decreased with the increase of Bi_2O_3 doping levels.

– The removal cross-sections have inverse effects with the addition Bi_2O_3 content, where the glass sample (S1) has a higher value ($\sum R = 0.173$ cm^{-1}).

– It is established that these glasses may contribute to the development of high-performance radiation shields.

The authors gratefully acknowledge the financial support and facility provided by the Department of Physics, College of Science, Mustansiriyah University, Iraq to complete this research work.

REFERENCES

1. S. Glasstone, A. Sesonske. *Nuclear Reactor Engineering: Reactor Design Basics.* Vol. 1. 4th edition (New York: Chapman & Hall, 1996) 464 p.
2. J.R. Lamarsh, A.J. Baratta. *Introduction to Nuclear Engineering.* 3rd edition (New Jersey: Prentice Hall, 2001) 783 p.
3. G.F. Knoll. *Radiation Detection and Measurement* (New York: John Wiley & Sons, 2010) 864 p.
4. K.A. Mahmoud et al. Investigation of radiation shielding properties for some building materials

reinforced by basalt powder. AIP Conf. Proc. 2174 (2019) 020036.
5. T.A. Taha, A.S. Abouhaswa. Preparation and optical properties of borate glass doped with MnO_2. J. Mater. Sci.: Mater. Electron. 29 (2018) 8100.
6. D.K. Gaikwad et al. Comparative study of gamma ray shielding competence of WO_3-TeO_2-PbO glass system to different glasses and concretes. Mater. Chem. Phys. 213 (2018) 508.
7. N. Chanthima, J. Kaewkhao. Investigation on radiation shielding parameters of bismuth borosilicate glass from 1 keV to 100 GeV. Ann. Nucl. Energy 55 (2013) 23.
8. S.F. Olukotun et al. Investigation of gamma radiation shielding capability of two clay materials. Nucl. Eng. Technol. 50(6) (2018) 957.
9. F. Akman et al. Determination of effective atomic numbers and electron densities from mass attenuation coefficients for some selected complexes containing lanthanides. Can. J. Phys. 95(10) (2017) 1005.
10. V.P. Singh et al. Determination of mass attenuation coefficient for some polymers using Monte Carlo simulation. Vacuum 119 (2015) 284.
11. M.I. Sayyed et al. Evaluation of shielding parameters for heavy metal fluoride based tellurite-rich glasses for gamma ray shielding applications. Radiat. Phys. Chem. 139 (2017) 33.
12. J. Singh et al. Fusible alloys: A potential candidate for gamma rays shield design. Prog. Nucl. Energy 106 (2018) 387.
13. R. Bagheri et al. Determination of gamma-ray shielding properties for silicate glasses containing Bi_2O_3, PbO, and BaO. J. Non-Cryst. Solids 479 (2018) 62.
14. M. Dong, B.O. Elbashir, M.I. Sayyed. Enhancement of gamma ray shielding properties by PbO partial replacement of WO_3 in ternary $60TeO_2$-(40-x)WO_3-xPbO glass system. Chalcogenide Lett. 14(3) (2017) 113.
15. S.A. Tijani et al. Radiation shielding properties of transparent erbium zinc tellurite glass system determined at medical diagnostic energies. J. Alloys Compounds 741 (2018) 293.
16. M. Kurudirek et al. Effect of Bi_2O_3 on gamma ray shielding and structural properties of borosilicate glasses recycled from high pressure sodium lamp glass. J. Alloys Compounds 745 (2018) 355.
17. M.I. Sayyed et al. Radiation shielding study of tellurite tungsten glasses with different antimony oxide as transparent shielding materials using MCNPX Code. J. Non-Cryst. Solids 498 (2018) 167.
18. S.B. Kolavekar et al. Optical, structural and Near-Ir NLO properties of gold nanoparticles doped sodium zinc borate glasses. Opt. Mater. 83 (2018) 34.
19. S. Mohan et al. Spectroscopic investigations of Sm^{3+}-doped lead alumino-borate glasses containing zinc, lithium and barium oxides. J. Alloys Compounds 763 (2018) 486.
20. M.I. Sayyed et al. ZnO-B_2O_3-PbO glasses: Synthesis and radiation shielding characterization. Physica B: Condensed Matter 548 (2018) 20.
21. I.O. Olarinoye. Photon buildup factors for some tissues and phantom materials for penetration depths up to 100 mfp. J. Nucl. Res. Dev. 13 (2017) 57.
22. Y. Harima. An historical review and current status of buildup factor calculations and applications. Radiat. Phys. Chem. 41(4-5) (1993) 631.
23. M.I. Sayyed et al. A comprehensive study of the energy absorption and exposure buildup factors of different bricks for gamma-rays shielding. Results Phys. 7 (2017) 2528.
24. S. Singh et al. Effect of finite sample dimensions and total scatter acceptance angle on the gamma ray buildup factor. Ann. Nucl. Energy 35(12) (2008) 2414.
25. S. Singh et al. Measurements of linear attenuation coefficients of irregular shaped samples by two media methods. Nucl. Instrum. Methods B 266(7) (2008) 1116.
26. A. Kumar et al. Effect of PbO on the shielding behavior of ZnO-P_2O_5 glass system using Monte Carlo simulation. J. Non-Cryst. Solids 481 (2018) 604.
27. M. Kurudirek, S. Topcuoglu. Investigation of human teeth with respect to the photon interaction, energy absorption and buildup factor. Nucl. Instrum. Methods B 269(10) (2011) 1071.
28. V.P. Singh, N.M. Badiger. Energy absorption buildup factors, exposure buildup factors and Kerma for optically stimulated luminescence materials and their tissue equivalence for radiation dosimetry. Radiat. Phys. Chem. 104 (2014) 61.
29. Y. Karabul et al. Computation of EABF and EBF for basalt rock samples. Nucl. Instrum. Methods A 797 (2015) 29.
30. H.C. Manjunatha, L. Seenappa. Pocket formula for mass attenuation coefficient, effective atomic number, and electron density of human tissues. Nucl. Sci. Tech. 30(3) (2019) 36.
31. M. Kurudirek. Photon buildup factors in some dosimetric materials for heterogeneous radiation sources. Radiat. Environ. Biophys. 53 (2014) 175.
32. M.F. Kaplan. *Concrete Radiation Shielding* (New York: John Wiley and Sons Inc., 1989) 448 p.
33. J. Wood. *Computational Methods in Reactor Shielding* (Oxford, Pergamon Press, 2013).
34. E. Şakar et al. Phy-X / PSD: Development of a user friendly online software for calculation of parameters relevant to radiation shielding and dosimetry. Radiat. Phys. Chem. 166 (2020) 108496.
35. V.F. Sears. Neutron scattering lengths and cross sections. Neutron News 3(3) (1992) 26.
36. P. Kaur et al. Investigation of bismuth borate glass system modified with barium for structural and gamma-ray shielding properties. Spectrochim. Acta A 206 (2019) 367.
37. K.A. Mahmoud et al. The role of cadmium oxides in the enhancement of radiation shielding capacities for alkali borate glasses. Ceram. Int. 46(15) (2020) 23337.
38. A.M. Abu El-Soad et al. Simulation studies for gamma ray shielding properties of Halloysite nanotubes using MCNP-5 code. Appl. Radiat. Isot. 154 (2019) 108882.

39. V.P. Singh, N.M. Badiger. Gamma ray and neutron shielding properties of some alloy materials. Ann. Nucl. Energy 64 (2014) 301.
40. H.C. Manjunatha, B. Rudraswamy. External bremsstrahlung spectra of the ^{90}Sr source in some lead compounds measured using NaI detector. Radiat. Meas. 47(1) (2012) 100.
41. V.P. Singh, N.M. Badiger. Shielding efficiency of lead borate and nickel borate glasses for gamma rays and neutrons. Glass Phys. Chem. 41 (2015) 276.
42. A. El Abd et al. A simple method for determining the effective removal cross section for fast neutrons. J. Radiat. Nucl. Appl. 2(2) (2017) 53.
43. M.H.A. Mhareb et al. Investigation of photon, neutron and proton shielding features of H_3BO_3-ZnO-Na_2O-BaO glass system. Nucl. Eng. Technol. 53(3) (2021) 949.
44. Y.S. Alajerami et al. Radiation shielding properties of bismuth borate glasses doped with different concentrations of cadmium oxides. Ceram. Int. 46(8) (2020) 12718.
45. P. Kaur et al. Investigation of a competent non-toxic Bi_2O_3-Li_2O-CeO_2-MoO_3-B_2O_3 glass system for nuclear radiation security applications. J. Non-Cryst. Solids 545 (2020) 120235.
46. J.F. Ziegler, M.D. Ziegler, J.P. Biersack. SRIM – The stopping and range of ions in matter (2010). Nucl. Instrum. Methods B 268(11-12) (2010) 1818.

Х. Абуд[1,*], І. Т. Аль-Алаві[1,2]

[1] Фізичний факультет, Науковий коледж, Університет Мустансірія, Багдад, Ірак
[2] Факультет медичної фізики, Коледж медичних технологій охорони здоров'я, Університет Аль-Шааб, Багдад, Ірак

*Відповідальний автор: han55608@yahoo.com

РАДІАЦІЙНИЙ ЗАХИСТ, ПОТУЖНІСТЬ ДОЗИ ТА ГАЛЬМІВНА ЗДАТНІСТЬ СИСТЕМИ КАДМІЙ - ВІСМУТ - СВИНЕЦЬ - ЦИНК - БОРАТНЕ СКЛО: ВПЛИВ ЛЕГУВАННЯ Bi_2O_3

Скляні системи виду (70-x)B_2O_3-10ZnO-10PbO-10CdO-xBi_2O_3 (з x = 0 до 20 моль%) були виготовлені стандартним методом з розплаву та охарактеризовані. Досліджено роль варіювання вмісту легуючої речовини Bi_2O_3 на радіаційне ослаблення, потужність дози та гальмівну здатність запропонованих стекол. Було оцінено різні характеристики захисту від радіації, такі як коефіцієнти накопичення експозиції, константи гамма-випромінювання та потужності дози, а також загальний поперечний переріз ослаблення нейтронів. Рентгенівська дифрактометрія зразків показала їхні аморфні характеристики. Щільність скла була збільшена з 5,34 до 6,95 г/см^3, а ширина забороненої зони зменшувалася зі збільшенням вмісту легуючої речовини Bi_2O_3. Крім того, як величини ослаблення, так і ефективні атомні числа зразків (розраховані за допомогою програмного забезпечення Phy-X) в діапазоні енергій гамма-променів від 0,015 до 15 МеВ збільшувались зі збільшенням вмісту Bi_2O_3. Зі збільшенням легування Bi_2O_3 було збільшено ослаблення гамма-променів, гальмівна здатність і поперечний переріз ослаблення нейтронів. Отримана нова скляна композиція є хорошим кандидатом для захисту від радіації.

Ключові слова: захист від гамма-випромінювання, боратне скло, нейтронні перерізи, параметри ослаблення.

Надійшла / Received 05.03.2024